Articles

IA_3, an Aspartic Proteinase Inhibitor from *Saccharomyces cerevisiae*, Is Intrinsically Unstructured in Solution†

Terry B. Green,‡ Omjoy Ganesh,‡ Kyle Perry,‡ Leif Smith,‡ Lowri H. Phylip,§ Timothy M. Logan,||,⊥ Stephen J. Hagen,@ Ben M. Dunn,‡ and Arthur S. Edison*,‡,⊥

Department of Biochemistry and Molecular Biology, Box 100245, University of Florida, Gainesville, Florida 32610-0245, School of Biosciences, Cardiff University, P.O. Box 911, Cardiff CF10 3US, Wales, United Kingdom, Department of Chemistry and Program in Molecular Biophysics, Florida State University, Tallahassee, Florida 32306, National High Magnetic Field Laboratory, 1800 East Paul Dirac Drive, Tallahassee, Florida 32310, and Department of Physics, Box 118440, University of Florida, Gainesville, Florida 32611-8440

Received May 19, 2003; Revised Manuscript Received January 9, 2004

ABSTRACT: IA_3 is a highly specific and potent 68-amino acid endogenous inhibitor of yeast proteinase A (YprA), and X-ray crystallographic studies have shown that IA_3 binds to YprA as an α-helix [Li, M., Phylip, L. H., Lees, W. E., Winther, J. R., Dunn, B. M., Wlodawer, A., Kay, J., and Gustchina, A. (2000) *Nat. Struct. Biol. 7*, 113−117]. Surprisingly, only residues 2−32 of IA_3 are seen in the X-ray structure, and the remaining residues are believed to be disordered in the complex. We have used circular dichroism (CD) and nuclear magnetic resonance (NMR) spectroscopy to show that IA_3 is unstructured in the absence of YprA. Specifically, IA_3 produced a CD spectrum characteristic of an unstructured peptide, and the ^{15}N HSQC NMR spectra of IA_3 were characteristic of a polypeptide lacking intrinsic structure. We characterized the unstructured state of IA_3 by using singular-value decomposition (SVD) to analyze the CD data in the presence of TFE, by fully assigning the unbound IA_3 protein by NMR and comparing the chemical shifts to published random-coil values, and by measuring $^1H-^{15}N$ heteronuclear NOEs, which are all consistent with an unfolded protein. The IA_3 samples used for NMR analyses were active and inhibited YprA with an inhibition constant (K_i) of 1.7 nM, and the addition of YprA led to a large spectral transition in IA_3. Calorimetric (ITC) data also show that the overall enthalpy of the interaction between IA_3 and YprA is exothermic.

IA_3, a 68-amino acid protein, is an endogenous, potent, and highly specific inhibitor of yeast proteinase A (YprA),[1] an aspartic proteinase from *Saccharomyces cerevisiae* (*1*). At least 15 related and structurally similar aspartic proteinases, including yeast yapsin 1, human pepsin, human gastricsin, human cathepsins D and E, and plasmepsin II from *Plasmodium falciparum*, are not inhibited by IA_3 and, in fact, cleave IA_3 as a substrate (*2*). The inhibition constant (K_i) for IA_3 inhibition of YprA catalysis is pH-dependent and ∼1−2 nM at pH 3.1, and IA_3 is not cleaved in the process (*2*, *3*). At higher pH values, the K_i is too small to accurately measure (*2*). The 34 N-terminal amino acids of IA_3 have the same potency as either the native IA_3 or recombinant IA_3 with a C-terminal Leu-Glu-$(His)_6$ tag (*2*).

The X-ray crystal structure of the YprA−IA_3 complex (*3*) is shown in Figure 1A. IA_3 forms a near-perfect α-helix in the active site cleft of YprA, an unprecedented mechanism of aspartic proteinase inhibition. Consistent with the functional data (*2*), only residues 2−32 from IA_3 form the α-helix (Figure 1B), and the 36 remaining C-terminal amino acids are not observed in the electron density (*3*). Despite numerous attempts, unbound IA_3 has not been crystallized (A. Wlodawer, personal communication), and the authors of the paper describing the YprA−IA_3 crystal structure (*3*) suggest that IA_3 is unstructured in the absence of YprA.

Relatively few protein inhibitors of aspartic proteinases have been identified (*2*). These include the renin-binding

† Supported by the University of Florida College of Medicine, the National High Magnetic Field Laboratory, BBSRC (72/C13544 to LHP), NIH (5P41RR016105-02 to ASE and IRO1AI4903-01 to BMD).

‡ Department of Biochemistry and Molecular Biology, University of Florida.

§ Cardiff University.

|| Florida State University.

⊥ National High Magnetic Field Laboratory.

@ Department of Physics, University of Florida.

[1] Abbreviations: YprA, yeast proteinase A; K_i, inhibition constant; NOE, nuclear Overhauser effect; PI-3, pepsin inhibitor-3; HSQC, heteronuclear single-quantum correlation; ITC, isothermal titration calorimetry; ΔH, calorimetric enthalpy; NMR, nuclear magnetic resonance; Nph, *p*-nitro-L-phenylalanine; NOESY, nuclear Overhauser effect (NOE) spectroscopy; TOCSY, total correlation spectroscopy; CD, circular dichroism; TFE, 2,2,2-trifluoroethanol; DSS, 2,2-dimethyl-2-silapentane-5-sulfonic acid; SDS−PAGE, sodium dodecyl sulfate−polyacrylamide gel electrophoresis; KH_2PO_4, potassium phosphate; WASP, Wiskott-Aldrich syndrome protein; UV, ultraviolet; SVD, singular-value decomposition.

10.1021/bi034823n CCC: $27.50
Published on Web 03/18/2004

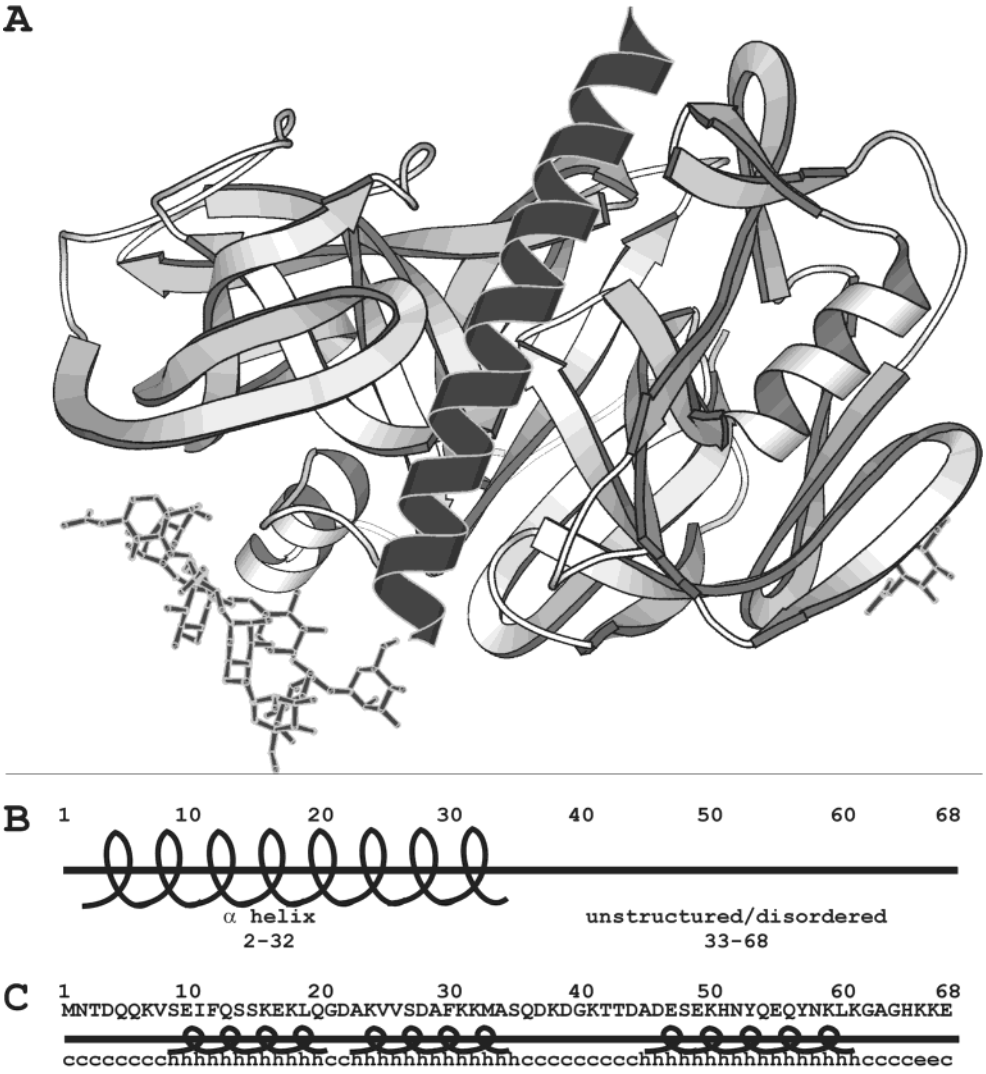

FIGURE 1: Representations of IA_3. (A) X-ray crystal structure of the YprA−IA_3 complex (*3*). Residues 2−32 of IA_3 are the dark α-helix running down the center of YprA, which is shown in lighter gray. YprA is glycosylated, as shown by the ball-and-stick structures. The drawing was prepared with Molscript (*49*). (B) Schematic representation of the secondary structure of IA_3 bound to YprA. Only residues 2−32, which form an α-helix (illustrated with a barrel), are seen in the crystal structure (*3*). (C) The GOR4 secondary structure program predicts that 62% of IA_3 will be in a helix.

protein (*4*), the *Ascaris lumbricoides* PI-3 pepsin and cathepsin E inhibitor (*5*), some plant proteins (*6*, *7*), and an inhibitor from sea anemone (*8*). Of these aspartic proteinase inhibitors, only the structures for YprA-bound IA_3 (*3*) and PI-3 (*9*) have been determined. Unlike IA_3, PI-3 was crystallized both free and in a complex with pepsin, and the mechanism of inhibition of PI-3 is completely different from those of both IA_3 and small molecule inhibitors (*9*). Thus, naturally occurring proteins have the potential to provide many new starting points for the design of novel inhibitors of aspartic proteinases.

Below, we present definitive proof that IA_3 is predominantly unstructured in the absence of YprA and demonstrate that the unstructured sample is fully active, inhibits YprA at nanomolar concentrations, and undergoes a large conformational transition upon binding to YprA. Thus, IA_3 is an example of the ever-growing list of intrinsically unstructured proteins that become structured only in the presence of a target binding partner (*10*). The fact that IA_3 inhibits YprA with such potency and specificity makes this unstructured-to-structured transition especially intriguing and provides an example of a ligand whose structures and dynamics play a key role in the regulation of its function.

MATERIALS AND METHODS

Sample Preparation. The IA_3 sample was prepared as previously described (*3*) with the substitution of M9 minimal medium [200 mL of 5X M9 salts (12.8 g of Na_2HPO_4, 3 g of KH_2PO_4, 0.5 g of NaCl, and 1.0 g of NH_4Cl), 2 mL of 1 M $MgSO_4$, 20 mL of 20% glucose, 100 μL of 1 M $CaCl_2$, and 777.9 mL of ddH_2O] with [^{13}C]glucose and [^{15}N]NH_4Cl (Cambridge Isotopes) as the sole nitrogen and carbon sources, respectively. The bacterial host strain for expression was BL21-CodonPlus (DE3) RIL competent cells (Stratagene). Cells were grown at 37 °C in M9 medium to an OD_{600} of ∼0.6 before induction with 1 mM IPTG. After expression had been carried out for 3 h, the cells were harvested by centrifugation and lysed by sonication. The soluble recombinant protein was purified using affinity chromatography followed by 10 min of boiling and centrifugation to remove nonsoluble material, as described by Li *et al.* (*3*). The protein was dialyzed in water before lyophilization.

Experimental Determination of K_i. Inhibition constants were determined with a kinetic assay using a chromogenic substrate with a Lys-Pro-Ile-Ala-Phe*Nph-Arg-Leu sequence. The asterisk indicates the cleavage site of the substrate. Changes in the maximum absorbance from 284 to 324 nm were recorded on a Hewlett-Packard 8452A diode array spectrometer. The temperature was controlled using a circulating water bath with insulation along the tubing leading into the cuvette holder; the temperature that was reported was recorded at the cuvette with a thermocouple probe. YprA (from 20 to 50 nM, depending on V_{max}), varying amounts of IA_3, and buffer [0.1 M sodium acetate (pH 4.5)] were incubated at the desired temperature for 5 min before mixing with various concentrations of the chromogenic substrate. For each temperature, initial rates of six different substrate concentrations (5, 10, 20, 40, 60, and 80 μM) were measured without IA_3 and with two different concentrations of IA_3 (e.g., 6.8 and 22.8 nM at 37 °C). The inhibition data were fitted to the Michaelis−Menten equation using Marquardt analysis. The inhibition constant (K_i) was fit using the equation

$$v = V_{max}/(1 + (K_m/[S]) \times (1 + [I]/K_i))$$

where v is the rate of the reaction, V_{max} is the maximum velocity, and [S] is the specific concentration of the substrate (molar). K_m is the substrate concentration at half the maximum velocity, and [I] is the inhibitor concentration (*11*).

Gel Filtration and Ion Exchange of YprA. Fifteen milligrams of YprA (Sigma) was dissolved into 600 μL of 20 mM KH_2PO_4 and 50 mM NaCl (pH 6.5) and loaded onto a Sephacryl (S-100) high-resolution column. Two peaks eluted from the column, and they both tested positive for YprA proteolytic activity. Stability tests were performed and analyzed in the presence of IA_3 at 4 and 22 °C. The results indicated that the first peak degraded IA_3 and the second peak did not at 4 °C. Therefore, the second peak from gel filtration was used in our studies. The fractions of the second peak were combined and loaded onto an Amersham Pharmacia Hi-trap Q ion exchange column at 4 °C. A gradient from 50 to 500 mM NaCl was used to elute the YprA off the ion exchange column. The fractions were tested for activity and combined to obtain a concentration of ~200 μM.

YprA−IA_3 Complex. A ~4-fold excess of IA_3 was added to the purified YprA before the mixture was concentrated to approximately 1 mL by ultrafiltration using an Amicon ultrafiltration cell [molecular weight cutoff (MWCO) of 3000]. The concentrated IA_3−YprA complex was then passed over a Sephacryl S-100 column. Two peaks (YprA−IA_3 complex and free IA_3) eluted from the column and were confirmed by SDS−PAGE analysis. Then, the fractions from the first peak were combined and concentrated by ultrafiltration (MWCO of 3000) to a final volume of ~570 μL in 20 mM KH_2PO_4 (pH 5.5) for NMR data collection. SDS−PAGE analysis was performed on the NMR sample after data were collected on the IA_3−YprA complex.

Circular Dichroism. Far-UV CD data were collected on an Aviv-202 circular dichroism spectrometer. IA_3 (~6 μM) was dissolved in deionized H_2O, and the cell path length, scan speed, and resolution were 1 mm, 0.5 nm/s, and 0.1 nm, respectively. To monitor temperature-dependent structural changes, CD data were collected at 5, 15, 25, 45, and 55 °C. Furthermore, a temperature scan from 5 to 65 °C using 3 °C increments was performed on IA_3 at 202 and 222 nm to observe temperature-dependent transitions. Trifluoroethanol (TFE) was added in 5% increments to ~30 μM IA_3 in water. To keep the concentration of IA_3 constant, a new sample was used for each TFE point using the same parameters described above.

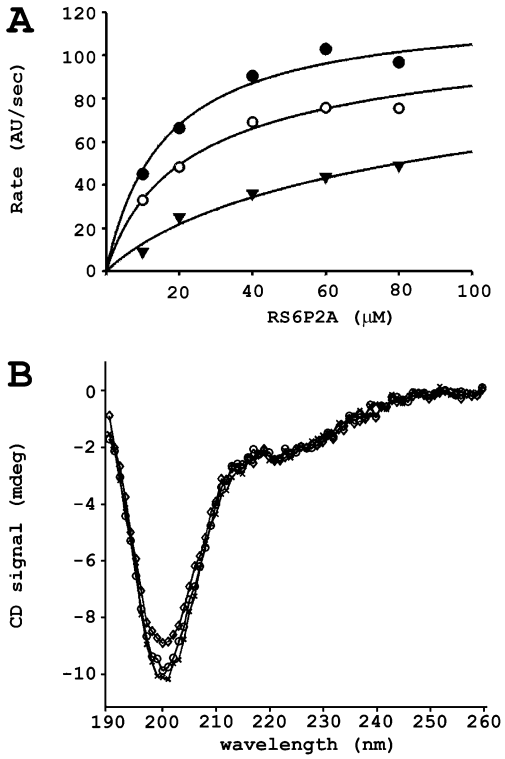

FIGURE 2: Biophysical studies of IA_3. (A) Recombinant IA_3 inhibits YprA. Recombinant IA_3 has a K_i of 1.7 nM (R^2 = 98%). The symbols represent the velocity of substrate cleavage in the presence of 0 (●), 6.8 (○), and 22.8 nM IA_3 (▼). (B) Far-UV CD spectra of recombinant IA_3 at 5 (×), 25 (○), and 55 °C (◇). The negative ellipticity at ~200 nm is characteristic of a disordered/unfolded protein.

Analysis of CD Spectra. We used singular-value decomposition (SVD) to analyze the CD spectra collected from the TFE titration (*12*). Briefly, the method generates a set of component spectra, $U_i(\lambda)$ (functions of wavelength), and associated amplitudes, SV_i(TFE) (functions of TFE concentration), that describe the evolution of the spectra as TFE is added. For the data in Figure 3A, the total matrix $A(\lambda,\text{TFE})$ of ellipticity values for different wavelengths (λ) and TFE concentrations at 25 °C can be decomposed as the sum of two contributions

$$A(\lambda,\text{TFE}) = SV_1(\text{TFE})\cdot U_1(\lambda) + SV_2(\text{TFE})\cdot U_2(\lambda)$$

Figure 3B shows the SV_1 and SV_2 amplitudes obtained from the decomposition, as a function of TFE. If the addition of TFE drives a two-state folding transition, then those amplitudes depend on the fraction of molecules folded, $[1 + \exp(-\Delta G/RT)]^{-1}$, and we can fit them as follows:

$$SV_1(\text{TFE}) = a_1 + b_1[1 + \exp(-\Delta G/RT)]^{-1}$$

$$SV_2(\text{TFE}) = a_2 + b_2[1 + \exp(-\Delta G/RT)]^{-1}$$

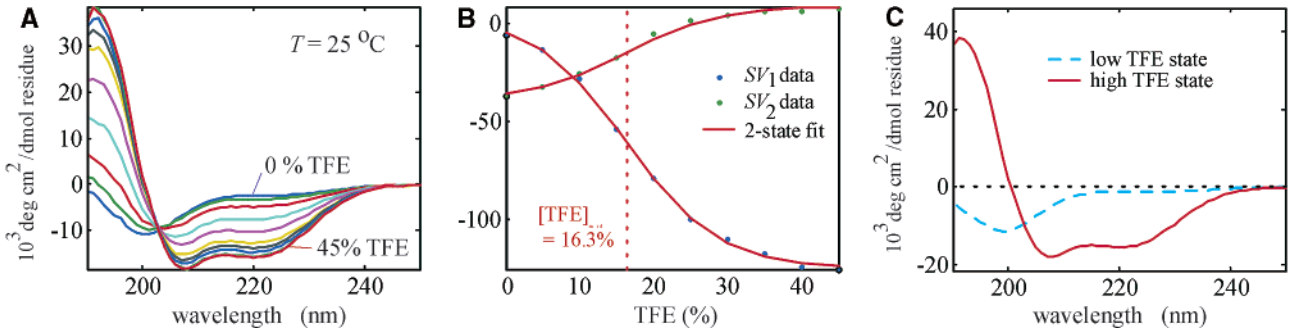

FIGURE 3: TFE titration of IA_3. (A) CD spectra for 0−45% TFE at 25 °C. (B) SVD analysis of CD spectral changes induced by TFE, including a fit to a two-state model. The transition midpoint is at 16.3% TFE (see Materials and Methods). (C) Basis states (derived from the SVD fit) corresponding to the low-TFE (blue) and high-TFE (red) states of IA_3.

where ΔG is the free energy of unfolding and a_1, a_2, b_1, and b_2 are constants. With the assumption that $\Delta G = \Delta G_0 + m$[TFE], the fit yields the values of ΔG_0 and m, along with the above constants. This fit gives the solid curves in Figure 3B. The CD spectra of the folded and unfolded basis states are then found by using the fit to extrapolate $A(\lambda,\text{TFE})$ toward large positive ΔG (folded state) or large negative ΔG (unfolded state):

$$\text{folded spectrum} = (a_1 + b_1)U_1 + (a_2 + b_2)U_2$$

$$\text{unfolded spectrum} = a_1U_1 + a_2U_2$$

These spectra are shown in Figure 3C.

NMR. Approximately 1 mM IA_3 was dissolved in a 90% H_2O/10% D_2O mixture with 50 mM phosphate buffer and 100 mM NaCl, and the pH was adjusted to 5.6. NMR data were collected at 600 and 750 MHz on Bruker Avance spectrometers in the Advanced Magnetic Resonance Imaging and Spectroscopy (AMRIS) facility at the University of Florida McKnight Brain Institute and at 720 MHz on a Varian Unity Plus spectrometer at the National High Magnetic Field Laboratory. Unless otherwise noted, NMR data were collected at 20 °C. All ^{1}H data were referenced to DSS (0.0 ppm), and ^{15}N and ^{13}C chemical shifts were indirectly referenced to DSS by multiplying the ^{1}H 0.0 Hz frequency by the ratios 0.101 329 118 and 0.251 449 530 to obtain the ^{15}N and ^{13}C 0.0 Hz frequencies, respectively (*13*). The chemical shift differences in Figure 5 were obtained using random-coil shifts determined in 8 M urea using Ac-G-G-X-G-G-NH_2 (*14*) and were corrected for sequence-dependent effects (*15*) using a Fortran program written by the authors.

All NMR data were obtained with the ^{1}H carrier frequency centered on water, which was eliminated using 3-9-19 watergate sequences (*16*). Two-dimensional ^{15}N HSQC (*16*, *17*) spectra were typically recorded with 10.0 ppm (2048 complex points) and 40.0 ppm (256 complex points) points in the ^{1}H and ^{15}N dimensions, respectively. The ^{1}H−^{15}N NOE (*18*) data were obtained with relaxation delay times of 5 s, in addition to the general parameters described above. Heteronuclear NOEs are reported as the ratios of the peak intensity with ^{1}H saturation to that without. Quadrature detection in all indirect dimensions was achieved using the States−TPPI method (*19*). All data were processed using NMRPipe (*20*) and analyzed with NMRView (*21*).

Sequential assignments were obtained manually according to standard methods utilizing current gradient-optimized versions of the following three-dimensional data sets: HNCO (*22*, *23*), HNCA (*22*, *23*), CBCA(CO)NH (*24*), CBCANH (*25*), ^{15}N TOCSY-HSQC (*26*, *27*), and HCC(CO)NH-TOCSY (*28*, *29*). The ^{15}N dimensions were typically recorded with the carrier at 116.6 ppm, a spectral width of 21 ppm, and 32 complex points. The ^{13}Cα/β dimensions were recorded with the carrier frequency at 42.5 ppm, a spectral width of 51 ppm, and 50 complex points. The ^{13}Cα dimensions were recorded with the carrier frequency at 56.8 ppm, a spectral width of 26.5 ppm, and 50 complex points. The ^{13}C′ dimensions were recorded with the carrier at 176 ppm, a spectral width of 10 ppm, and 30 complex points.

The IA_3−YprA complex was prepared as described above at a concentration of ~200 μM. The complex sample is unstable at room temperature but can be kept for extended periods of time at 4 °C. Because of the low concentration, we used a Bruker 5 mm triple-resonance cryoprobe, which has a lower temperature limit of 10 °C. Therefore, ^{15}N HSQC experiments were carried out on the cryoprobe at 10 °C. As shown in Results, these data yielded two distinct types of peaks, large and broad peaks in the unfolded region of the spectrum and a second set of smaller and more dispersed peaks. We therefore recorded ^{15}N TROSY (*30*) spectra at 720 MHz on a Varian Unity Plus spectrometer at the National High Magnetic Field Laboratory. TROSY experiments were carried out at a range of temperatures, from 4 to 20 °C. However, there were no significant differences between the HSQC and 720 MHz TROSY data, and below we present only the HSQC data because they had a higher signal-to-noise ratio.

Isothermal Calorimetry (ITC). Calorimetric data were collected using a VP-ITC microcalorimeter from Microcal (Northhampton, MA). IA_3 and YprA were exchanged into 0.1 M sodium acetate (pH 4.5). IA_3 was injected into a sample cell containing ~0.5 μM YprA at 25 °C. The experiment consisted of 59 injections of a 15 μM stock solution of IA_3. The first injection, 1 μL, was deleted from the analysis (*31*). The subsequent injections were 5 μL each and were made over the course of 10 s with 4 min intervals between ensuing injections. The contents of the sample cell were stirred at 460 rpm to ensure proper mixing of both solutions. Control experiments to determine the heat of dilution were carried out by titrating IA_3 into the sample cell containing only buffer and by averaging the heat obtained per injection after saturation of YprA by IA_3. The heats of dilution for control injections were averaged and subtracted from each injection of the binding experiment.

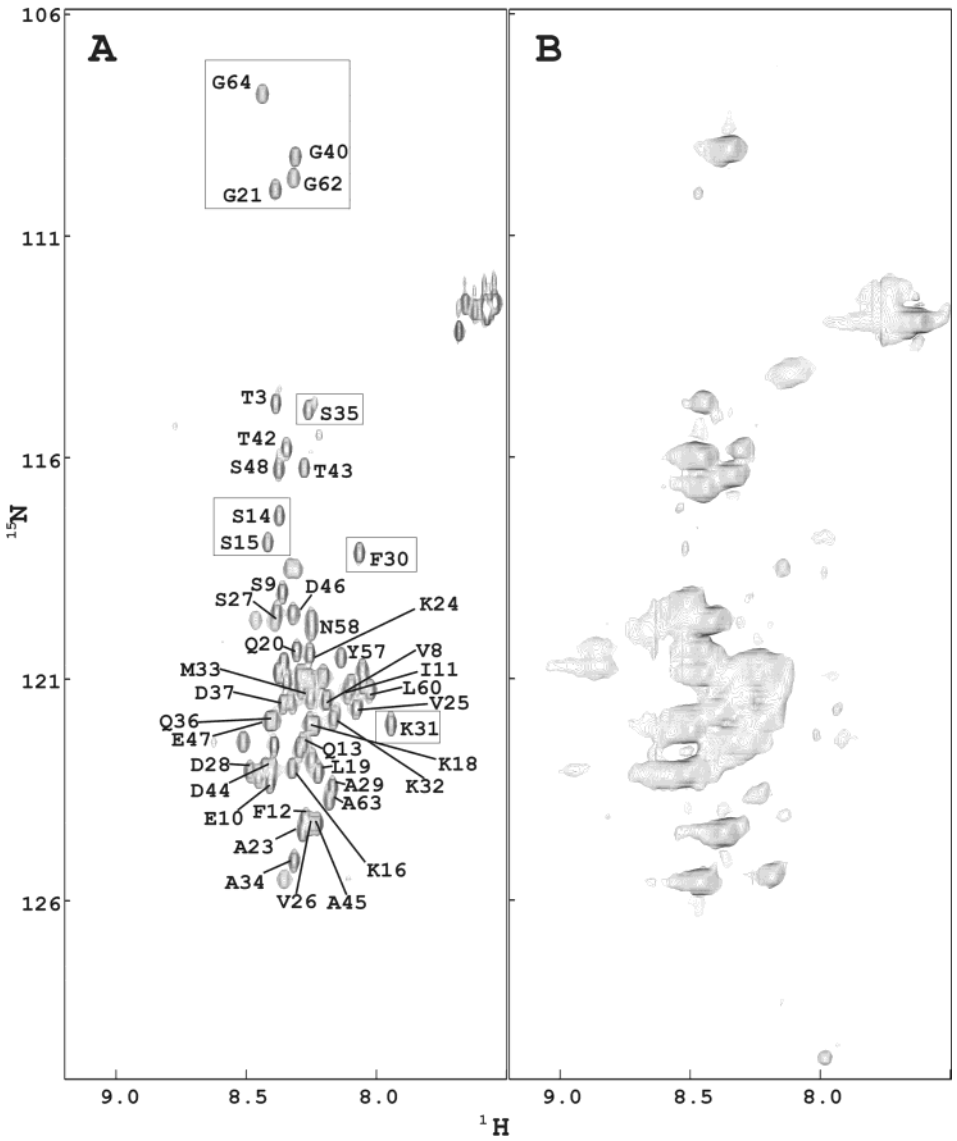

FIGURE 4: IA_3 undergoes large conformational changes upon binding of YprA. Both panels are ^{15}N HSQC spectra of ^{15}N-labeled IA_3 recorded under various conditions: (A) free IA_3 at 20 °C and (B) gel-filtered IA_3−YprA complex with unlabeled YprA at 10 °C. Resolved residues (S14, S15, G21, K30, K31, S35, G40, G62, and G64) in the free IA_3 that obviously shift in the YprA complex are boxed. The many small peaks that appear in the IA_3−YprA complex are believed to be the result of the N-terminal residues undergoing a transition to an α-helix as seen in the crystal structure.

The data were analyzed using Origin (OriginLab, Northampton, MA). Each injection generates a peak in the power supplied to the sample. The area under the peak is equivalent to the heat released from the sample, and integration of the series of peaks generates the binding isotherm. The binding isotherm was deconvoluted by well-established methods (*32*), and a Levenberg−Marquardt nonlinear least-squares fitting method was then used to generate a best fit of the data and determine $\Delta H°$ (enthalpy), K_a (association constant), and n (number of binding sites). The binding affinity of IA_3 for YprA is very strong, so the K_a determined from ITC is not accurate and was not used in our analysis (*31*, *33*).

RESULTS

IA_3 Lacks Stable Structure in Solution. IA_3 inhibits YprA with a K_i value of 1.7 nM (Figure 2A). Circular dichroism (Figure 2B) was used to analyze the secondary structure of IA_3 at 5, 15, 25, 45, and 55 °C. Unstructured proteins give rise to CD spectra with a negative band near 200 nm and some weak bands (positive or negative) between 220 and 230 nm (*34*). α-Helical proteins typically show double minima at 222 and 208−210 nm and a maximum at 191−193 nm (*34*). Although Figure 2B shows a slight inflection around 222 nm that may represent a very small amount of α-helix, the CD spectrum of IA_3 is characteristic of an unfolded protein with a strong minimum peak at ∼200 nm for all of the above temperatures. These data indicate that recombinant IA_3 is a predominantly unstructured active inhibitor whose structure is temperature-independent over the range of 5−55 °C.

Although the CD data illustrate that free IA_3 is unstructured, the addition of 2,2,2-trifluoroethanol (TFE) to the solvent induces a helical state in the protein. Figure 3A shows the mean residue ellipticity for IA_3 at 25 °C as the TFE concentration increases from 0 to 45% in steps of 5%. The appearance of an isodichroic point near 203 nm clearly shows

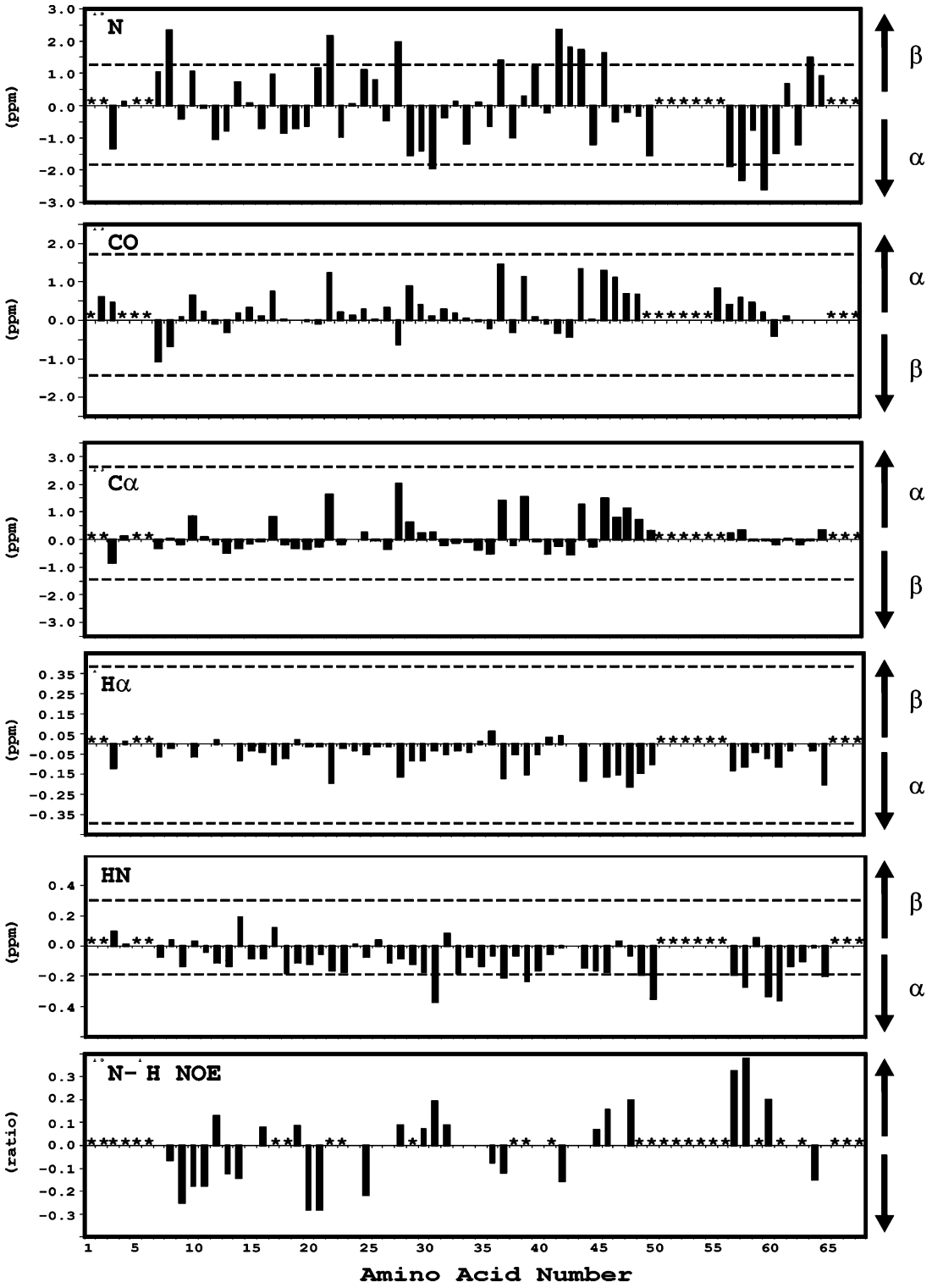

FIGURE 5: Deviations from random-coil chemical shifts and $^1H-^{15}N$ NOEs for uncomplexed IA_3. Regions marked with asterisks were not assigned due to extensive overlap and ambiguities. The top five panels are δ(exp) − δ(random coil) in parts per million for different nuclei. The random-coil shifts were those determined in 8 M urea using Ac-G-G-X-G-G-NH_2 (*14*) and were corrected for sequence-dependent effects (*15*). The average secondary shifts for an α-helix and *β*-strand relative to random-coil values (*37*) are indicated by dashed lines on each panel. The $^1H-^{15}N$ NOEs (*18*) on the bottom panel are the ratios of the peak intensity with ^1H saturation to that without.

a two-state transition. A minimum develops near 222 nm, indicating that the rising TFE concentration stabilizes α-helical structure in the peptide. Although the stabilization of helical structure by TFE is a well-known phenomenon (*35*), the data in Figure 3A qualitatively verify that IA_3 is unfolded in the absence of TFE and allow us to determine the energetics of helix formation in IA_3. We performed singular-value decomposition (SVD) of these spectra (*12*) and fit that decomposition to a two-state folding−unfolding model (see Materials and Methods), under the assumption that the free energy of unfolding, ΔG, increases linearly with TFE concentration ($\Delta G = \Delta G_0 + m$[TFE]). This fit gives a ΔG_0 of −6.50 kJ/mol and an m of 0.40 kJ mol^{-1} (% TFE)$^{-1}$ at 25 °C.

Thus, the fit indicates a free energy of unfolding equal to −6.50 kJ/mol in the absence of TFE at room temperature, or that 93% of the molecules are unfolded under these conditions. The folding midpoint occurs at $\Delta G = 0$, or 16.3% TFE. The SVD analysis also gives the CD spectra of the folded (high TFE) and unfolded (low TFE) states (Figure 3C). The unfolded state spectrum shows the minimum near 200 nm, typical of a disordered protein [∼6−8% helical by CDPro analysis (*36*)], while the folded state shows the distinct minimum near 222 nm, characteristic of an α-helix [∼50% helix by CDPro (*36*)]. Therefore, the far-UV CD strongly indicates that the addition of TFE to the solvent drives IA_3 from an initially disordered state to a largely helical conformation, through a two-state transition.

The ^{15}N HSQC NMR spectrum of free IA_3 in solution is characteristic of an unfolded protein (Figure 4A). When another ^{15}N-labeled IA_3 sample was lyophilized and resuspended in 100% D_2O, all of the amide peaks exchanged before we could collect a ^1H one-dimensional spectrum (<3 min, data not shown). An equal volume of 100% H_2O was then added to the deuterium-exchanged sample, and the resulting sample produced an HSQC spectrum similar to that shown in Figure 4A (data not shown). These results suggest that free IA_3 is unstructured and show that all of the amide protons are highly accessible to solvent.

NMR chemical shifts are sensitive indicators of protein secondary structure (reviewed, for example, in ref *37*). Although proteins with 60−70 amino acids can often be assigned from ^1H NMR data alone, the ^1H NMR spectra of IA_3 were hopelessly overlapped. We next tried to assign the protein using just three-dimensional (3D) ^{15}N-based methods, but even these spectra were too overlapped to yield more than ∼20% of the assignments. Therefore, we produced a doubly labeled (^{13}C and ^{15}N) IA_3 sample and used 3D ^{15}N TOCSY-HSQC and HC(CO)NH-TOCSY experiments that were originally developed for assigning unfolded proteins (*29*). These experiments were supplemented by other standard triple-resonance data sets to obtain nearly complete backbone and partial side chain assignments for IA_3 free in solution. The backbone chemical shifts are analyzed below, and the side chain shifts are almost all average values. The NMR assignments were deposited in the BioMagResBank (accession number 6078).

Figure 5 shows deviations from random-coil values for ^{15}N, $^1H^N$, $^1H^\alpha$, $^{13}C^\alpha$, and $^{13}C'$ chemical shifts. The experimental data were referenced to DSS. The reference values were obtained from a study of random-coil shifts in 8 M urea (*14*) and corrected for sequence-dependent effects (*15*) as described in Materials and Methods. Although we were unable to assign a region from residue 51 to 56 due to extensive overlap, the chemical shifts suggest a region of a moderately populated α-helix near the C-terminus from approximately D44 through L60. GOR IV (*38*) and AGADIR (*39*, *40*) both predict several regions of α-helix in IA_3 as indicated in Figure 1C. NMR data are consistent with that prediction in the C-terminus, but the helix is not substantially populated experimentally. Although the N-terminal half of IA_3 has been shown to bind to YprA as an α-helix, experimental results in the absence of YprA indicate that the IA_3 N-terminus is predominantly unstructured.

An unstructured protein should also have significant flexibility in solution (*41*). Therefore, we measured heteronuclear $^1H-^{15}N$ NOEs (*18*) on [^{15}N]IA_3 (Figure 5). As expected for an unfolded protein, all of the NOEs in IA_3 are very small (<0.3) or negative, clearly indicating that the protein is disordered in solution. Thus, chemical shifts and NOEs provide quantitative verification of the CD data shown above and demonstrate that IA_3 is primarily unstructured and flexible in its unbound state.

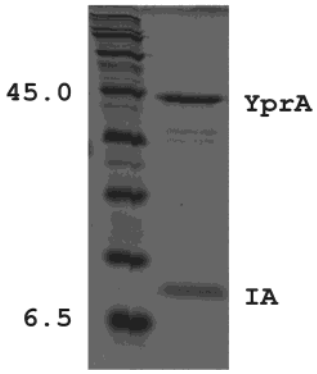

FIGURE 6: SDS−PAGE analysis of the IA_3−YprA complex. Bio-Rad SDS Broad Range Standards in kilodaltons (lane 1) and the IA_3−YprA complex (lane 2) were run on a 15% SDS−polyacrylamide gel and stained with Coomassie Blue. One microliter of the IA_3−YprA complex was taken directly from the NMR tube following the NMR titration to check for degradation of IA_3. The complex sample was maintained at 10 °C throughout the course of the NMR experiments and frozen when not in use.

IA_3 Undergoes a Structural Transition in the Presence of YprA. Upon binding to YprA, IA_3 undergoes a significant conformational change. The $^{15}N-^1H$ HSQC spectrum of the IA_3−YprA complex (Figure 4B) is largely different from the spectrum of free IA_3 (Figure 4A). The glycine resonances (G21, G40, G62, and G64), which are well-resolved in free IA_3, shift to a different frequency or disappear in the IA_3−YprA complex. Several resolved resonances in the YprA binding region (e.g., S14, 15, F30, and K31) disappear or shift to another frequency in the IA_3−YprA complex. In addition, 36 new resolved, but small, resonances appear in the IA_3−YprA complex spectrum that are not seen in the free IA_3 spectrum. We interpret these shifts as evidence of IA_3 undergoing a conformational change to an α-helix as seen in the X-ray structure.

An SDS−PAGE gel of the NMR sample (Figure 6) was run after the NMR data in Figure 4B were collected to check for proteolysis of the IA_3−YprA complex. The gel showed two bands the size of YprA and IA_3. We cannot rule out the possibility of a small amount of partial proteolysis, but our data suggest that most, if not all, of the IA_3 in the complex was intact.

Stability studies (data not shown) on the IA_3−YprA complex indicate that it degrades within less than 3 days at room temperature, perhaps due to slow exchange of the bound and free IA_3 or to contaminating proteases in the sample. Therefore, the NMR data shown in Figure 4B were collected at 10 °C. The molecular mass of the complex is more than 50 kDa, and as a result of the low temperature, the correlation time of this sample is expected to be very long. As a result, the ^{15}N HSQC spectrum of the complex has two very different types of peaks, approximately half that are strong and broadened with little chemical shift dispersion and half that are small and more dispersed. They are present in approximately equal numbers, consistent with

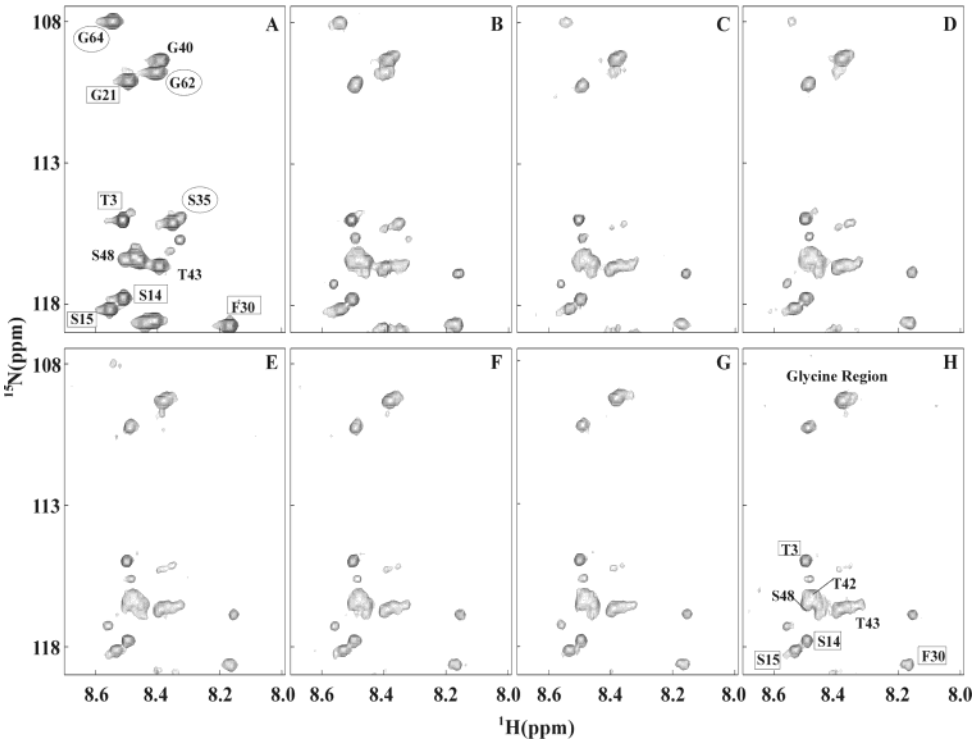

FIGURE 7: IA_3−YprA titration. Unlabeled YprA (~0.15 mM) was added in 5−40 μL increments to 550 μL of 0.4 mM ^{15}N-labeled IA_3. As the sample volume exceeded 800 μL, it was concentrated back to 550 μL. Roughly 50 ^{15}N HSQC spectra were collected in this titration, and eight which span the concentration ranges are shown here. The expansions show the glycine and serine/threonine regions of the HSQC spectra. Circled residues disappear, and boxed residues lose intensity but are not completely gone by the end of the titration. The residues remaining in this region are relatively unaffected. Approximate concentrations of IA_3 and YprA (in micromolar) are as follows: (A) 400 and 0.0, (B) 400 and 122, (C) 400 and 129, (D) 370 and 134, (E) 340 and 139, (F) 320 and 143, (G) 310 and 145, and (H) 300 and 147, respectively.

the fact that only the N-terminal half of the IA_3 polypeptide chain binds directly to YprA. We collected ^{15}N TROSY data at 720 MHz on the same complex and obtained data remarkably similar to those of the HSQC spectrum shown in Figure 4B. The similarity between the two experiments could result from a number of factors, including dynamics, proton dipolar interactions (YprA is fully protonated), or low magnetic field strength.

We were surprised to see that three of the IA_3 glycine residues (G40, G62, and G64) that are outside of the YprA binding domain were significantly changed between panels A and B of Figure 4. This observation, along with the broadness of the large peaks in Figure 4B, made us suspect intermediate chemical exchange. Therefore, we also conducted a partial titration of YprA into a sample of [^{15}N]IA_3 (Figure 7). The titration was continued up to an IA_3:YprA ratio of ~2:1, and we collected ^{15}N HSQC spectra at several points. The peaks from the N-terminal half of IA_3 that are known to be involved in YprA binding decreased in intensity, as expected. However, the unexpected result was that the three glycine residues and at least one additional resolved resonance, S35, in the noninteracting portion of IA_3 disappeared at substoichiometric amounts of YprA. This behavior was consistent with data in Figure 4B on the stoichiometric complex and suggests that residues in the C-terminus of IA_3 are in intermediate exchange in the presence of YprA.

The Binding of IA_3 to YprA Is Exothermic. Taken together, the data presented above and the X-ray crystal structure (*3*) demonstrate that IA_3 folds upon binding to YprA. Therefore, the thermodynamics of inhibition should reflect both the protein folding and ligand binding events. We measured the enthalpy of IA_3 binding and folding to YprA by ITC analysis.

Figure 8 shows results from ITC studies in which IA_3 was titrated into YprA. The reaction is clearly exothermic with a ΔH of -86.0 ± 3.0 kJ/mol (-20.6 ± 0.7 kcal/mol). ITC is unable to accurately determine association constants for tight-binding ligands such as binding of IA_3 to YprA (*31*, *33*). Therefore, we were unable to obtain values of ΔG or ΔS using only ITC.

DISCUSSION

In this study, we have shown that active IA_3 is predominantly unstructured in solution by CD and NMR analysis but undergoes a large structural transition upon binding to YprA. Previous work has shown that (1) IA_3 is exquisitely specific for YprA and is degraded as a substrate by other closely related aspartic proteinases (*2*), (2) the first 32 amino acids of IA_3 bind to YprA as an α-helix (*3*), (3) the 34 N-terminal residues account for all of the inhibitory activity of IA_3 (*2*), and (4) many mutations in these 34 residues produce little or no decrease in the level of binding (*2*). The α-helix formed by IA_3 when bound to YprA is amphipathic, with primarily hydrophobic residues plus a single serine on the YprA side of the helix and polar or charged groups facing the solvent (*3*). Thus, it is not surprising that IA_3 could not form a stable helix as a monomer in aqueous solution, even over a broad range of temperatures. In addition, we have also shown that IA_3 will form a stable helix in the presence of TFE.

Although we have not yet assigned NMR resonances of the IA_3−YprA complex, our data provide new insights into

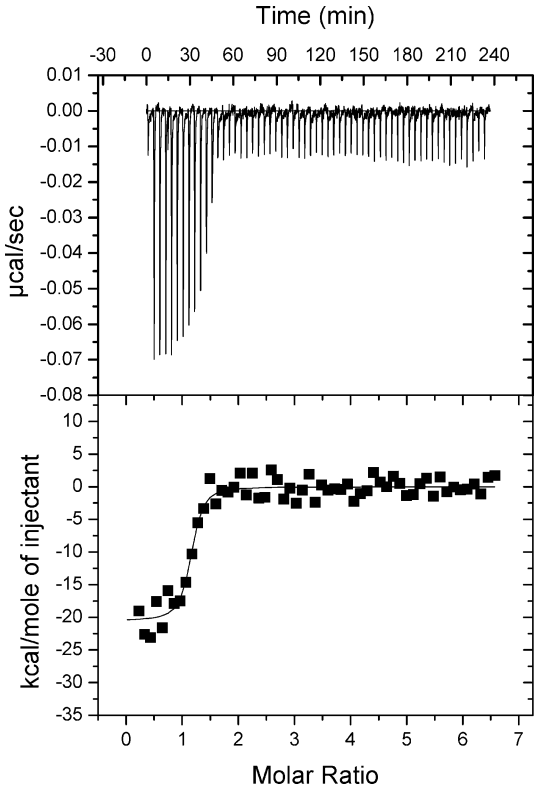

FIGURE 8: Isothermal calorimetry data for binding of IA_3 to YprA. The experiment consisted of 59 injections of a 15 μM IA_3 stock solution into YprA. The first injection was 1 μL, and subsequent injections were 5 μL. The top panel shows the power supplied to the sample cell (relative to a water reference cell) during the injection series, to maintain a constant temperature of 25 °C. The integrated area under the curve gives the heat released per mole of IA_3 added (bottom panel). A fit to the data indicates a binding enthalpy ΔH of -86.0 ± 3.0 kJ/mol (-20.6 ± 0.7 kcal/mol). The heat of dilution was determined from the data after saturation (i.e., after ~50 min in the top panel) and has been subtracted from the isotherm.

the interactions of IA_3 with YprA. We have conclusively shown that IA_3 alone has very little structure in solution. The resonances of IA_3 shift significantly upon addition of YprA, showing that IA_3 undergoes a structural transition. The regions with the glycines, serines, and threonines are very informative. For example, the glycine region contains four resolved resonances (G21, G40, G62, and G64) without any YprA added. On the basis of the crystal structure and inhibition data, we would expect G21 to change but the others to be unaffected by YprA. However, in the IA_3-YprA complex, all of the glycine resonances change. The YprA titration data provide some evidence that the glycine residues outside the YprA binding region are in intermediate chemical exchange, because the peaks vanish at YprA concentrations well below stoichiometric YprA concentrations. It is unlikely that this could arise from YprA degradation of IA_3 given that SDS−PAGE results show pure bands for both IA_3 and YprA following collection of NMR data. The IA_3 residues involved in binding to YprA appear to be in slow exchange by virtue of the fact that they decrease in intensity monotonically with the titration as new peaks corresponding to the bound structure increase in intensity. Finally, by examining both the bound complex (Figure 4B) and the YprA titration (Figure 7), we can identify several residues whose chemical shifts appear to be relatively unaffected by YprA: T42, T43, and S48.

Many of the resolved IA_3 resonances (e.g., S14, S15, F30, K31, and S35) disappear in the IA_3-YprA complex. These results are not unexpected, because most of these are located in IA_3's electron density of the IA_3-YprA complex. The first 34 residues are known to be involved in the inhibition (*2*). Serine 35 is just outside of the electron density observed in the crystal structure of the IA_3-YprA complex. However, it is not surprising that this residue is affected by YprA binding, because it might either represent a frayed end of the α-helix or simply be extremely constricted by YprA binding.

The interpretation most consistent with the data for the IA_3-YprA complex is that the N-terminus of IA_3 is binding tightly to YprA and undergoing slow exchange. This produces the 36 small peaks that are in the complex spectrum but absent in the free spectrum. In contrast, the C-terminus of IA_3 is interacting with YprA and undergoing a rather complicated exchange between free and bound states. Some of the residues must be in rather fast exchange or have little contact with YprA, because there are approximately 34 large but broadened peaks in the HSQC spectrum of the complex. However, some peaks, like the three C-terminal glycine residues, appear to vanish upon addition of a small amount of YprA, and this is most consistent with intermediate exchange behavior.

We measured the K_i of binding of IA_3 to YprA to be 3.0 nM at 25 °C, from which we can estimate a binding free energy of −49 kJ/mol (−11.7 kcal/mol) using the equation $\Delta G = -RT \ln K_i$. However, because the interaction between IA_3 and YprA involves folding as well as binding and inhibition, a two-state description clearly oversimplifies the process. An accurate thermodynamic analysis of the interaction will require measurement of the separate entropic and enthalpic contributions to each stage of the interaction, through calorimetric and other studies of IA_3 and its variants, together with quantitative modeling. Such studies are in progress, and we anticipate they will lead to a clearer picture of the energetics of this complex interaction.

At least one other yeast aspartic proteinase, yapsin, cleaves but is not inhibited by IA_3, and it is known from truncation studies with IA_3 that the proteolytically cleaved products are inactive as inhibitors of YprA (*2*). How does IA_3 escape being cleaved by YprA? The NMR and CD data of IA_3 show only a very small percentage of α-helix in solution, and NMR chemical shifts show that the helix is localized to the C-terminal half of the protein. Our biophysical data support the model in which YprA forms a unique template upon which IA_3 folding is catalyzed. We have not yet determined the kinetics of IA_3 binding to YprA or the complete thermodynamic details of the binding of each half of IA_3.

Numerous examples of intrinsically unfolded proteins folding into structural proteins exist in the recent literature (*10*, *42*−*45*), although to our knowledge IA_3 is the first identified intrinsically unfolded proteinase inhibitor. Unfolded proteins play major roles in transcriptional (*46*, *47*) and translational activation (*48*), cytoskeleton formation and restructuring (*49*), signal transduction (*50*), membrane transport/signaling (*51*), and cell-cycle control (*52*−*54*). For example, the activation domain of transcription factor CREB and the acid activation domains of p53 and VP16 fold into

amphipathic helical structures upon binding to CBP, MDM2, and TAFII31, respectively (*10*). Studies on the intrinsically unstructured GTPase-binding domain of WASP have demonstrated that it can form different structures, depending on the context of the interactions (*49*). The p27 protein, which is intrinsically disordered in solution and a member of the p21 family of Cdk inhibitors, folds into an ordered structure that comprises an α-helix, a 3_{10}-helix, and β-structure when bound to the cyclin A-Cdk2 (*54*). IA_3 is yet another example in the field of unstructured/disordered proteins that folds when it recognizes its target. IA_3 is produced in yeast and inhibits yeast proteinase A, so there is an obvious need to regulate the activity of IA_3. We can speculate that perhaps the unfolded state of IA_3 allows for post-translational regulation of its activity.

ACKNOWLEDGMENT

The valuable contributions of John Kay (School of Biosciences, Cardiff University) and Alexander Wlodawer and Alla Gustchina (National Cancer Institute, Frederick, MD) to this work are greatly appreciated. Geoffrey Gordon kindly assisted with CD studies.

REFERENCES

1. Dreyer, T., Valler, M. J., Kay, J., Charlton, P., and Dunn, B. M. (1985) The selectivity of action of the aspartic-proteinase inhibitor IA3 from yeast (*Saccharomyces cerevisiae*), *Biochem. J. 231*, 777−779.
2. Phylip, L. H., Lees, W. E., Brownsey, B. G., Bur, D., Dunn, B. M., Winther, J. R., Gustchina, A., Li, M., Copeland, T., Wlodawer, A., and Kay, J. (2001) The potency and specificity of the interaction between the IA3 inhibitor and its target aspartic proteinase from *Saccharomyces cerevisiae*, *J. Biol. Chem. 276*, 2023−2030.
3. Li, M., Phylip, L. H., Lees, W. E., Winther, J. R., Dunn, B. M., Wlodawer, A., Kay, J., and Gustchina, A. (2000) The aspartic proteinase from *Saccharomyces cerevisiae* folds its own inhibitor into a helix, *Nat. Struct. Biol. 7*, 113−117.
4. Takahashi, S., Takahashi, K., Kaneko, T., Ogasawara, H., Shindo, S., Saito, K., and Kobayashi, M. (1999) Identification of cysteine-380 as the essential residue for the human *N*-acetyl-D-glucosamine 2-epimerase (renin binding protein), *J. Biochem. 126*, 639−642.
5. Kageyama, T. (1998) Molecular cloning, expression and characterization of an *Ascaris* inhibitor for pepsin and cathepsin E, *Eur. J. Biochem. 253*, 804−809.
6. Kreft, S., Ravnikar, M., Mesko, P., Pungercar, J., Umek, A., Kregar, I., and Strukelj, B. (1997) Jasmonic acid inducible aspartic proteinase inhibitors from potato, *Phytochemistry 44*, 1001−1006.
7. Christeller, J. T., Farley, P. C., Ramsay, R. J., Sullivan, P. A., and Laing, W. A. (1998) Purification, characterization and cloning of an aspartic proteinase inhibitor from squash phloem exudate, *Eur. J. Biochem. 254*, 160−167.
8. Lenarcic, B., and Turk, V. (1999) Thyroglobulin type-1 domains in equistatin inhibit both papain-like cysteine proteinases and cathepsin D, *J. Biol. Chem. 274*, 563−566.
9. Ng, K. K., Petersen, J. F., Cherney, M. M., Garen, C., Zalatoris, J. J., Rao-Naik, C., Dunn, B. M., Martzen, M. R., Peanasky, R. J., and James, M. N. (2000) Structural basis for the inhibition of procine pepsin by *Ascaris* pepsin inhibitor-3, *Nat. Struct. Biol. 7*, 653−657.
10. Wright, P. E., and Dyson, H. J. (1999) Intrinsically unstructured proteins: re-assessing the protein structure−function paradigm, *J. Mol. Biol. 293*, 321−331.
11. Dunn, B. M., Scarborough, P. E., Davenport, R., and Swietnicki, W. (1994) Analysis of proteinase specificity by studies of peptide substrates. The use of UV and fluorescence spectroscopy to quantitate rates of enzymatic cleavage, *Methods Mol. Biol. 36*, 225−243.
12. Henry, E. R., and Hofrichter, J. (1992) Singular value decomposition: Application to analysis of experimental data, *Methods Enzymol. 210*, 129−192.
13. Wishart, D. S., Bigam, C. G., Holm, A., Hodges, R. S., and Sykes, B. D. (1995) ^1H, ^{13}C and ^{15}N random coil NMR chemical shifts of the common amino acids. Investigations of nearest-neighbor effects, *J. Biomol. NMR 5*, 67−81.
14. Schwarzinger, S., Kroon, G. J., Foss, T. R., Wright, P. E., and Dyson, H. J. (2000) Random coil chemical shifts in acidic 8 M urea: implementation of random coil shift data in NMRView, *J. Biomol. NMR 18*, 43−48.
15. Schwarzinger, S., Kroon, G. J., Foss, T. R., Chung, J., Wright, P. E., and Dyson, H. J. (2001) Sequence-dependent correction of random coil NMR chemical shifts, *J. Am. Chem. Soc. 123*, 2970−2978.
16. Piotto, M., Saudek, V., and Sklenar, V. (1992) Gradient-tailored excitation for single-quantum NMR spectroscopy of aqueous solutions, *J. Biomol. NMR 2*, 661−665.
17. Bodenhausen, G., and Ruben, D. J. (1980) Natural abundance N-15 NMR by enhanced heteronuclear spectroscopy, *Chem. Phys. Lett. 69*, 185−189.
18. Farrow, N. A., Muhandiram, R., Singer, A. U., Pascal, S. M., Kay, C. M., Gish, G., Shoelson, S. E., Pawson, T., Forman-Kay, J. D., and Kay, L. E. (1994) Backbone dynamics of a free and phosphopeptide-complexed Src homology 2 domain studied by ^{15}N NMR relaxation, *Biochemistry 33*, 5984−6003.
19. Marion, D., Ikura, M., Tschudin, R., and Bax, A. (1989) Rapid recording of 2D NMR spectra without phase cycling. Application to the study of hydrogen exchange in proteins, *J. Magn. Reson. 85*, 393−399.
20. Delaglio, F., Grzesiek, S., Vuister, G. W., Zhu, G., Pfeifer, J., and Bax, A. (1995) NMRPipe: a multidimensional spectral processing system based on UNIX pipes, *J. Biomol. NMR 6*, 277−293.
21. Johnson, B. A., and Bax, A. (1994) NMRView: A computer program for the visualization and analysis of NMR data, *J. Biomol. NMR 4*, 603−614.
22. Grzesiek, S., and Bax, A. (1992) Improved 3D triple-resonance NMR techniques applied to a 31-kDa protein, *J. Magn. Reson. 96*, 432−440.
23. Kay, L. E., Ikura, M., Tschudin, R., and Bax, A. (1990) Three-dimensional triple-resonance NMR spectroscopy of isotopically enriched proteins, *J. Magn. Reson. 89*, 496−514.
24. Grzesiek, S., and Bax, A. (1992) Correlating backbone amide and side-chain resonances in larger proteins by multiple relayed triple resonance NMR, *J. Am. Chem. Soc. 114*, 6291−6293.
25. Grzesiek, S., and Bax, A. (1992) An efficient experiment for sequential backbone assignment of medium-sized isotopically enriched proteins, *J. Magn. Reson. 99*, 201−207.
26. Marion, D., Driscoll, P. C., Kay, L. E., Wingfield, P. T., Bax, A., Gronenborn, A. M., and Clore, G. M. (1989) Overcoming the overlap problem in the assignment of ^1H NMR spectra of larger proteins by use of three-dimensional heteronuclear $^1H-^{15}N$ Hartmann−Hahn-multiple quantum coherence and nuclear Overhauser-multiple quantum coherence spectroscopy: application to interleukin-1β, *Biochemistry 28*, 6150−6156.
27. Palmer, A. G., Cavanagh, J., Wright, P. E., and Rance, M. (1991) Sensitivity improvement in proton-detected two-dimensional heteronuclear correlation NMR spectroscopy, *J. Magn. Reson. 93*, 151−170.
28. Lyons, B. A., and Montelione, G. T. (1993) An HCCNH triple-resonance experiment using C-13 isotropic mixing for correlating backbone amide and side-chain aliphatic resonances in isotopically enriched proteins, *J. Magn. Reson., Ser. B 101*, 206−209.
29. Logan, T. M., Olejniczak, E. T., Xu, R. X., and Fesik, S. W. (1993) A general method for assigning NMR spectra of denatured proteins using 3D HC(CO)NH-TOCSY triple resonance experiments, *J. Biomol. NMR 3*, 225−231.
30. Pervushin, K., Riek, R., Wider, G., and Wuthrich, K. (1997) Attenuated T-2 relaxation by mutual cancellation of dipole−dipole coupling and chemical shift anisotropy indicates an avenue to NMR structures of very large biological macromolecules in solution, *Proc. Natl. Acad. Sci. U.S.A. 94*, 12366−12371.
31. Pierce, M. M., Raman, C. S., and Nall, B. T. (1999) Isothermal titration calorimetry of protein−protein interactions, *Methods 19*, 213−221.
32. Jelesarov, I., and Bosshard, H. R. (1999) Isothermal titration calorimetry and differential scanning calorimetry as complementary tools to investigate the energetics of biomolecular recognition, *J. Mol. Recognit. 12*, 3−18.

33. Holdgate, G. A. (2001) Making cool drugs hot: Isothermal titration calorimetry as a tool to study binding energetics, Drug Discovery and Genomic Technologies, *BioTechniques 31*, 164−186.
34. Woody, R. W. (1995) Circular dichroism, *Methods Enzymol. 246*, 34−71.
35. Buck, M. (1998) Trifluoroethanol and colleagues: cosolvents come of age. Recent studies with peptides and proteins, *Q. Rev. Biophys. 31*, 297−355.
36. Sreerama, N., and Woody, R. W. (2000) Estimation of protein secondary structure from circular dichroism spectra: comparison of CONTIN, SELCON, and CDSSTR methods with an expanded reference set, *Anal. Biochem. 287*, 252−260.
37. Wishart, D. S., and Sykes, B. D. (1994) Chemical shifts as a tool for structure determination, *Methods Enzymol. 239*, 363−392.
38. Garnier, J., Gibrat, J. F., and Robson, B. (1996) GOR method for predicting protein secondary structure from amino acid sequence, *Methods Enzymol. 266*, 540−553.
39. Munoz, V., and Serrano, L. (1995) Elucidating the folding problem of helical peptides using empirical parameters. III. Temperature and pH dependence, *J. Mol. Biol. 245*, 297−308.
40. Munoz, V., and Serrano, L. (1995) Elucidating the folding problem of helical peptides using empirical parameters. II. Helix macrodipole effects and rational modification of the helical content of natural peptides, *J. Mol. Biol. 245*, 275−296.
41. Farrow, N. A., Zhang, O., Forman-Kay, J. D., and Kay, L. E. (1997) Characterization of the backbone dynamics of folded and denatured states of an SH3 domain, *Biochemistry 36*, 2390−2402.
42. Dyson, H. J., and Wright, P. E. (2002) Coupling of binding and folding for unstructured proteins, *Curr. Opin. Struct. Biol. 12*, 54−60.
43. Tompa, P. (2002) Intrinsically unstructured proteins, *Trends Biochem. Sci. 27*, 527−533.
44. Dunker, A. K., Brown, C. J., Lawson, J. D., Iakoucheva, L. M., and Obradovic, Z. (2002) Intrinsic disorder and protein function, *Biochemistry 41*, 6573−6582.
45. Dunker, A. K., Obradovic, Z., Romero, P., Garner, E. C., and Brown, C. J. (2000) Intrinsic protein disorder in complete genomes, *Genome Inf. Ser. 11*, 161−171.
46. Parker, D., Rivera, M., Zor, T., Henrion-Caude, A., Radhakrishnan, I., Kumar, A., Shapiro, L. H., Wright, P. E., Montminy, M., and Brindle, P. K. (1999) Role of secondary structure in discrimination between constitutive and inducible activators, *Mol. Cell. Biol. 19*, 5601−5607.
47. Daughdrill, G. W., Chadsey, M. S., Karlinsey, J. E., Hughes, K. T., and Dahlquist, F. W. (1997) The C-terminal half of the anti-sigma factor, FlgM, becomes structured when bound to its target, sigma 28, *Nat. Struct. Biol. 4*, 285−291.
48. Fletcher, C. M., and Wagner, G. (1998) The interaction of eIF4E with 4E-BP1 is an induced fit to a completely disordered protein, *Protein Sci. 7*, 1639−1642.
49. Kim, A. S., Kakalis, L. T., Abdul-Manan, N., Liu, G. A., and Rosen, M. K. (2000) Autoinhibition and activation mechanisms of the Wiskott-Aldrich syndrome protein, *Nature 404*, 151−158.
50. He, X. L., Chow, D. C., Martick, M. M., and Garcia, K. C. (2001) Allosteric activation of a spring-loaded natriuretic peptide receptor dimer by hormone, *Science 293*, 1657−1662.
51. Pfander, R., Neumann, L., Zweckstetter, M., Seger, C., Holak, T. A., and Tampe, R. (1999) Structure of the active domain of the herpes simplex virus protein ICP47 in water/sodium dodecyl sulfate solution determined by nuclear magnetic resonance spectroscopy, *Biochemistry 38*, 13692−13698.
52. Kriwacki, R. W., Hengst, L., Tennant, L., Reed, S. I., and Wright, P. E. (1996) Structural studies of p21Waf1/Cip1/Sdi1 in the free and Cdk2-bound state: conformational disorder mediates binding diversity, *Proc. Natl. Acad. Sci. U.S.A. 93*, 11504−11509.
53. Adkins, J. N., and Lumb, K. J. (2002) Intrinsic structural disorder and sequence features of the cell cycle inhibitor p57Kip2, *Proteins 46*, 1−7.
54. Bienkiewicz, E. A., Adkins, J. N., and Lumb, K. J. (2002) Functional consequences of preorganized helical structure in the intrinsically disordered cell-cycle inhibitor p27(Kip1), *Biochemistry 41*, 752−759.

BI034823N